Article

Developmental Cell

Modulation of Ciliary Phosphoinositide Content Regulates Trafficking and Sonic Hedgehog Signaling Output

Graphical Abstract

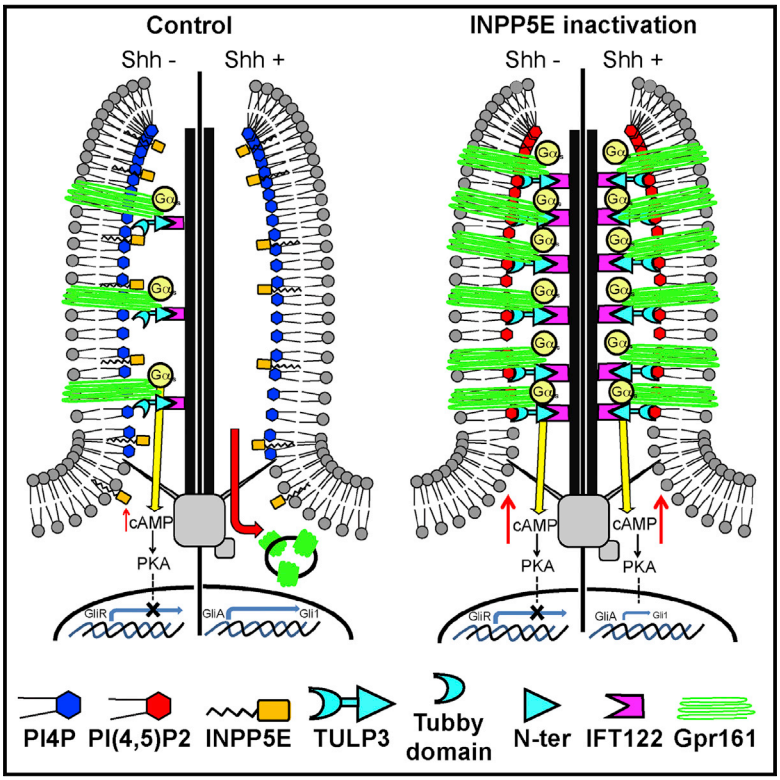

Highlights

- PI4P is the main PIP in NSC primary cilia, whereas PI(4,5)P2 is not detectable
- PI(4,5)P2 accumulates in cilia upon INPP5E inactivation with PI4P depletion
- TULP3 and the Shh repressor Gpr161 accumulate in cilia upon INPP5E inactivation
- INPP5E inactivation results in reduced DG neurogenesis and Shh signaling in NSCs

Authors

Marcelo Chávez, Sabrina Ena, Jacqueline Van Sande, Alban de Kerchove d'Exaerde, Stéphane Schurmans, Serge N. Schiffmann

Correspondence

echavez@ulb.ac.be (M.C.), sschiffm@ulb.ac.be (S.N.S.)

In Brief

Chávez et al. identify the main phosphoinositide species in neural stem cell primary cilia and show that the PIP phosphatase INPP5E regulates their levels. Loss of INPP5E changes the dominant cilium phosphoinositide species and affects recruitment of the PIP-interacting protein TULP3 and its cargo Gpr161, with effects on Shh signaling.

Chávez et al., 2015, Developmental Cell *34*, 338–350
August 10, 2015 ©2015 Elsevier Inc.
http://dx.doi.org/10.1016/j.devcel.2015.06.016

CellPress

Developmental Cell
Article

Modulation of Ciliary Phosphoinositide Content Regulates Trafficking and Sonic Hedgehog Signaling Output

Marcelo Chávez,[1,*] Sabrina Ena,[1] Jacqueline Van Sande,[2] Alban de Kerchove d'Exaerde,[1] Stéphane Schurmans,[3] and Serge N. Schiffmann[1,*]

[1]Laboratory of Neurophysiology, ULB Neuroscience Institute, Université Libre de Bruxelles (ULB), Brussels 1070, Belgium
[2]IRIBHM, Université Libre de Bruxelles, Brussels 1070, Belgium
[3]Laboratory of Functional Genetics, GIGA Research Centre, and WELBIO, Université de Liège, Liège 4000, Belgium
*Correspondence: echavez@ulb.ac.be (M.C.), sschiffm@ulb.ac.be (S.N.S.)
http://dx.doi.org/10.1016/j.devcel.2015.06.016

SUMMARY

Ciliary transport is required for ciliogenesis, signal transduction, and trafficking of receptors to the primary cilium. Mutations in inositol polyphosphate 5-phosphatase E (INPP5E) have been associated with ciliary dysfunction; however, its role in regulating ciliary phosphoinositides is unknown. Here we report that in neural stem cells, phosphatidylinositol 4-phosphate (PI4P) is found in high levels in cilia whereas phosphatidylinositol (4,5)-bisphosphate (PI(4,5)P2) is not detectable. Upon INPP5E inactivation, PI(4,5)P2 accumulates at the ciliary tip whereas PI4P is depleted. This is accompanied by recruitment of the PI(4,5)P2-interacting protein TULP3 to the ciliary membrane, along with Gpr161. This results in an increased production of cAMP and a repression of the Shh transcription gene Gli1. Our results reveal the link between ciliary regulation of phosphoinositides by INPP5E and Shh regulation via ciliary trafficking of TULP3/Gpr161 and also provide mechanistic insight into ciliary alterations found in Joubert and MORM syndromes resulting from INPP5E mutations.

INTRODUCTION

Cilia are hair-like structures emerging from most cells (Berbari et al., 2009). Primary cilia are sensory organelles wherein components of different signaling pathways concentrate (Berbari et al., 2009). For instance, essential constituents of Sonic Hedgehog (Shh) signaling such as Patched, Gli proteins, Smo, and suppressor of fused and regulators such as Gpr161 concentrate in primary cilia (Mukhopadhyay et al., 2013; Rohatgi et al., 2007). Neural stem cells (NSCs) possess a primary cilium, which detects Shh signaling for their postnatal establishment, expansion, and regional specification (Han et al., 2008; Ihrie et al., 2011; Lai et al., 2003). Epidermal growth factor receptor and platelet-derived growth factor receptor alpha are also expressed on primary cilia of NSCs and neuroblasts (Danilov et al., 2009).

Phosphoinositides (PIPs) are known to play major physiological roles in different cellular compartments (Balla, 2013), and data linking PIPs to primary cilium function have been reported (Franco et al., 2014; Vieira et al., 2006; Wei et al., 2008). The tubby family proteins share a C-terminal tubby domain, which interacts selectively with certain PIPs (Mukhopadhyay and Jackson, 2011; Mukhopadhyay et al., 2010; Santagata et al., 2001). One member of this family, the Tubby-like protein 3 (TULP3), traffics a subset of G protein-coupled receptors (GPCRs) including Gpr161, a negative Shh regulator (Mukhopadhyay et al., 2013), into the primary cilium (Mukhopadhyay et al., 2010). A group of ciliopathy patients with Joubert and MORM syndromes presents mutations in inositol polyphosphate 5-phosphatase E (INPP5E) (Bielas et al., 2009; Jacoby et al., 2009), an enzyme that removes the 5-phosphate from phosphatidylinositol (4,5)-bisphosphate (PI(4,5)P2) and phosphatidylinositol (3,4,5)-trisphosphate (PI(3,4,5)P3) (Dyson et al., 2012). Although these studies point to the relevance of different PIPs and PIP-interacting proteins in ciliary homeostasis and function, no direct evidence of PIPs has been reported in the ciliary compartment so far, and their regulation and function in primary cilia remain largely unknown.

In this study, we identify the main PIPs in primary cilia of NSCs and demonstrate that their levels are regulated by INPP5E. We describe how PI(4,5)P2 accumulates in cilia upon INPP5E inactivation, leading to accumulation of TULP3 and Gpr161 and subsequent repression of Shh response. In vivo, INPP5E inactivation resulted in ciliary alterations and reduced neurogenesis in the hippocampal dentate gyrus (DG), where Shh signaling, acting through the primary cilia, has a critical role in the expansion of postnatal progenitors (Breunig et al., 2008; Han et al., 2008).

Thus, our results provide a molecular link between PIP regulation at the ciliary membrane and Shh signaling.

RESULTS

INPP5E Inactivation Results in Increased Cycling and AKT Activation in Proliferating NSCs In Vitro

To gain insight into the ciliary regulation of PIPs by INPP5E in NSCs, we first looked for INPP5E expression. When cells from the brain subventricular zone are exposed to epidermal growth factor (EGF) in serum-free conditions in vitro, they grow to form floating cellular clusters known as neurospheres, which are self-renewing (Doetsch et al., 2002). Upon EGF removal and by adding

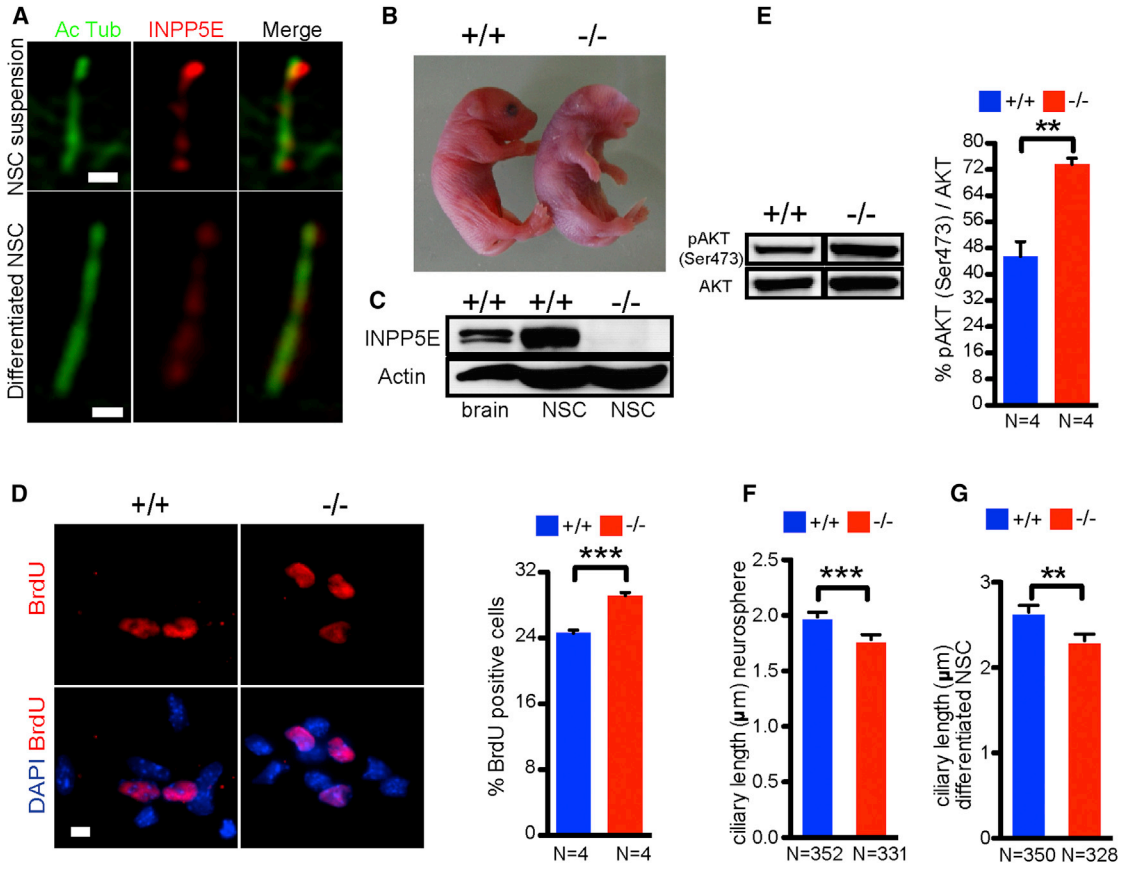

Figure 1. Effects of INPP5E Inactivation on Proliferating and Differentiated Neural Stem Cells In Vitro

(A) Immunostaining for INPP5E expression in proliferating NSCs in suspension and differentiated NSCs. The scale bars represent 500 nm.

(B) E18.5 *INPP5E*$^{+/+}$ and anophthalmic *INPP5E*$^{-/-}$ embryos.

(C) Western blots for INPP5E of control brain and cultured *INPP5E*$^{+/+}$ and *INPP5E*$^{-/-}$ NSCs.

(D) BrdU incorporation in cultured *INPP5E*$^{+/+}$ and *INPP5E*$^{-/-}$ NSCs in proliferating conditions after a 1-hr BrdU pulse; between 1,000 and 4,500 cells per culture coming from four different NSC cultures were counted and scored for BrdU incorporation by counterstaining with DAPI. Unpaired t test, mean ± SEM, ***p < 0.0001. The scale bar represents 5 μm.

(E) Western blotting for AKT phosphorylation on cultured *INPP5E*$^{+/+}$ and *INPP5E*$^{-/-}$ NSCs in proliferating conditions (N, number of independent cultures for each genotype). Unpaired t test, mean ± SEM, **p = 0.001.

(F) Ciliary length in proliferating NSCs. Mann-Whitney test, mean ± SEM, ***p < 0.0001.

(G) Ciliary length in differentiated NSCs. Mann-Whitney test, mean ± SEM, **p < 0.001.

See also Figures S1 and S2.

serum, neurospheres differentiate into neurons, astrocytes, and oligodendrocytes (Doetsch et al., 1999). Using an antibody against INPP5E (Jacoby et al., 2009), we found that INPP5E is expressed in the primary cilium of both proliferating and differentiated NSCs (Figure 1A). We next sought to identify the effects of INPP5E inactivation in NSCs by crossing heterozygous *INPP5E*$^{+/-}$ mice and harvesting and culturing NSCs from brains at embryonic day (E)18.5, because full inactivation of INPP5E is lethal perinatally (Jacoby et al., 2009). At this age, homozygous embryos were readily identifiable by anophthalmia (Jacoby et al., 2009) (Figure 1B). INPP5E inactivation in mouse embryonic fibroblasts leads to an increased number of cells in S and G2/M phases upon serum stimulation (Jacoby et al., 2009). Consistent with that report, we found that *INPP5E*$^{-/-}$ NSCs exhibited a significant increase in proliferation as detected by bromodeoxyuridine (BrdU) incorporation, which labels cells in S phase (Figure 1D).

INPP5E hypomorphic mutations have been reported to lead to increased AKT activation (Bielas et al., 2009). Consistently, we found that *INPP5E*$^{-/-}$ NSCs presented an increased AKT phosphorylation (Figure 1E), presumably due to an increase of PI(3,4,5)P3, which is one of the INPP5E substrates (Dyson et al., 2012) and an activator of AKT (Balla, 2013). Whereas pAKT has been reported to be located beneath the cilium of cortical progenitors (Higginbotham et al., 2013), PI(3,4,5)P3 localization in the cilium is not known. We checked for pAKT and PI(3,4,5)P3 in neurospheres by immunostaining and found pAKT distributed diffusely within the cells (Figure S1A). However, we could not detect pAKT within cilia in either control neurospheres or upon INPP5E inactivation (Figure S1A, magnified panels). An anti-PI(3,4,5)P3 antibody revealed the reported localization of PI(3,4,5)P3 at the plasma membrane (Kwon et al., 2010; Niswender et al., 2003; Tao et al., 2010) (Figure S1B). However,

we could not detect PI(3,4,5)P3 within cilia in either wild-type or mutant cells (Figure S1B, magnified panels). These results suggest that the increased phosphorylation of AKT, likely due to increased PI(3,4,5)P3 levels, probably takes place outside the cilia, when cilia are disassembled during the cell cycle (Kobayashi and Dynlacht, 2011).

We next examined the effect of INPP5E inactivation on ciliary length and found that there was a reduction in primary cilium length in neurospheres, a difference that persisted after cell differentiation (Figures 1F and 1G). Although neurospheres contain rapidly cycling cells (Doetsch et al., 2002) the resulting differentiated cells are mostly postmitotic (Jensen and Parmar, 2006), suggesting that the reduction in length in *INPP5E*$^{-/-}$ cells is likely due to intrinsic effects on ciliary length rather than to cell-cycle reentry. Together, and consistent with previous reports (Bielas et al., 2009), these results show that under proliferating conditions, INPP5E inactivation leads to an increased proliferation and an increased AKT phosphorylation, likely due to accumulation of the INPP5E substrate PI(3,4,5)P3.

Conditional Inactivation of INPP5E Results in Ciliary Alterations with Reduced Hippocampal Neurogenesis In Vivo

To assess the role of INPP5E postnatally in NSCs in vivo, we generated a conditional mouse using the human glial fibrillary acidic protein (hGFAP) promoter, which drives recombination of floxed alleles in NSCs (Han et al., 2008). NSCs known as type I progenitors continue to generate new granule neurons in the adult hippocampal DG (Seri et al., 2001). To assess production of neurons in the DG, we injected adult mice intraperitoneally with BrdU and found a reduction in BrdU incorporation in the DG of *hGFAP-Cre;INPP5E*$^{flox/-}$ mice (Figures S2A–S2C).

We also found that primary cilia in cells of the DG granular layer presented dilatation at the ciliary tip (Figures S2D–S2I), an alteration that is associated with defective retrograde intraflagellar transport in other cell types (Wei et al., 2012). To understand the mechanisms behind these alterations in the DG, we cultured NSCs from control and *hGFAP-Cre;INPP5E*$^{flox/-}$ mice in adherent conditions (see Experimental Procedures). Cells were grown until confluence and then starved to induce ciliation. Most of the cultured cells expressed the NSC marker nestin and the astrocyte cell marker GFAP (not shown). Control cells expressed INPP5E in primary cilia (Figure S3A). Similar to proliferating NSCs, we found a reduction in ciliary length in *hGFAP-Cre;INPP5E*$^{flox/-}$ cells compared to control cultures (Figure S3C), whereas there was no difference in the percentage of ciliated cells between both cultures (Figure S3B). Adherent NSCs formed longer cilia (Figure S3C) than NSCs in suspension (Figure 1F), growing apart from the cellular body, and were therefore preferred for characterization of mechanisms behind ciliary alterations upon INPP5E inactivation.

INPP5E Inactivation Leads to Ciliary Accumulation of PI(4,5)P2 with PI4P Depletion

To explore the possible link between INPP5E phosphatase activity and the alterations found in vitro (Figure 1) and in vivo (Figure S2) upon INPP5E inactivation, we searched for INPP5E targets and products at the ciliary membrane by using high-resolution confocal microscopy and anti-PIP antibodies validated to identify PIPs in different compartments (Hammond et al., 2009) and at the plasma membrane (PM) (Hammond et al., 2006, 2012). Whereas most PI(4,5)P2 is found at the PM (Watt et al., 2002) (Figure S4A), we could not detect PI(4,5)P2 at the ciliary membrane in control cells (N = 28) (Figure 2A; Figure S4A, top panels).

In contrast, PI(4,5)P2 was detectable in cilia upon INPP5E inactivation in *hGFAP-Cre;INPP5E*$^{flox/-}$ cells (Figure 2B; Figure S4A, bottom panels). Interestingly, in these cells, PI(4,5)P2 followed a gradient toward the ciliary tip covering 62.47% ± 3.49% (mean ± SEM, N = 33) of the distal part of the cilia. This distribution extended in a continuous manner or a spotty pattern along the ciliary axoneme covering 4.5% of the distal part of all cilia, whereas it was absent in 6.4% of the ciliary base in all cilia (Figures 2B and 2C). Reexpression of the wild-type form of INPP5E in *Cre;INPP5E*$^{flox/-}$ cells successfully prevented PI(4,5)P2 ciliary accumulation (Figures 2D and 2E). To test whether that effect was dependent on the enzymatic activity of INPP5E, we introduced a point mutation into INPP5E by substituting aspartic acid at position 477 for an asparagine, thus rendering INPP5E enzymatically null (Kong et al., 2006). This phosphatase-dead form of INPP5E, D477N, failed to prevent PI(4,5)P2 accumulation (Figures 2F and 2G), thus showing that INPP5E enzymatic activity is required to prevent ciliary accumulation of PI(4,5)P2.

PI(4,5)P2 staining was specific, as it was abolished by neomycin, known to bind PI(4,5)P2 with high affinity (Hammond et al., 2006) (Figure S5A).

PI(4,5)P2 is found at the PM along with phosphatidylinositol 4-phosphate (PI4P) (Balla, 2013), where both appear to provide the PM with a negative electrostatic charge (Hammond et al., 2012). PI(4,5)P2 hydrolysis by INPP5E results in PI4P. We found that PI4P was present in primary cilia from control cultures (Figure 3A; Figure S4B, upper panels) and, strikingly, it was depleted from primary cilia in *hGFAP-Cre;INPP5E*$^{flox/-}$ cells (Figures 3A and 3B; Figure S4B, bottom panels). In control cilia, PI4P was continuously distributed along the ciliary axoneme, covering 87.33% ± 1.22% (mean ± SEM, N = 19) of the distal part of the cilia, and absent in 4% of the ciliary base of all cilia (Figure 3C). PI4P staining was confirmed to be specific, because it was abolished by incubating an anti-PI4P antibody with 1-palmitoyl-2-oleoyl-*sn*-glycero-3-phosphocholine (POPC) liposomes containing PI4P but not with POPC liposomes alone (Hammond et al., 2009) (Figure S5B).

Lipid gradients in membranes are the result of localized production (Kim et al., 2013), impeded diffusion (Zhang et al., 2012), or asymmetrical degradation (Balla, 2013). We wondered whether PI(4,5)P2 accumulation at the ciliary tip upon INPP5E inactivation could be explained by a localized production of PI(4,5)P2. Although no PIP kinase has been identified in the ciliary proteome (Ishikawa et al., 2012), we found that the mouse PIP5Kγ isoform PIP5K1C was enriched at the base of cilia and not at the tip of the ciliary axoneme, as would have been expected in the case of asymmetric PI(4,5)P2 production (Figure S6A). Thus, it appears that PI(4,5)P2 accumulation at the ciliary tip is the direct consequence of the nondegradation by INPP5E and/or an impeded diffusion within the ciliary compartment. The mutant form of INPP5E found in patients with

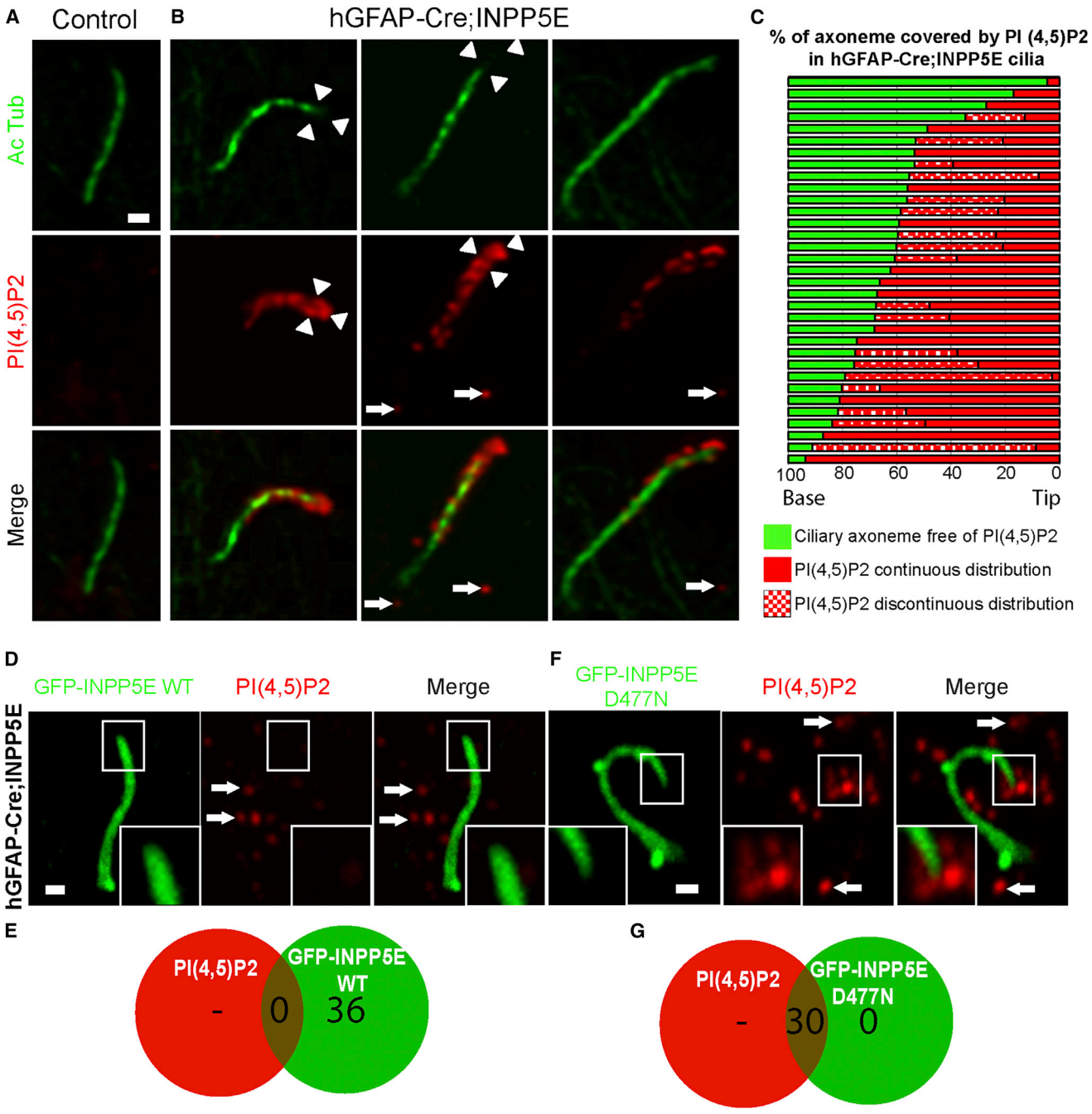

Figure 2. PI(4,5)P2 Regulation in Primary Cilia of Adherent NSCs

(A and B) Immunofluorescence for PI(4,5)P2 in (A) control and (B) *hGFAP-Cre;INPP5E*$^{flox/-}$ NSC cultures.

(C) Quantification of the percentage of the ciliary axoneme covered by PI(4,5)P2 in *hGFAP-Cre;INPP5E*$^{flox/-}$ cultures. Each bar represents a cilium (N = 33).

(D) Reexpression of GFP-INPP5E WT in *hGFAP-Cre;INPP5E*$^{flox/-}$ cultures.

(E) Venn diagram depicting the absence of overlap between GFP-INPP5E WT cilia (N = 36) and PI(4,5)P2.

(F) Expression of GFP-INPP5E D477N in *hGFAP-Cre;INPP5E*$^{flox/-}$ cultures.

(G) Venn diagram depicting the overlap between GFP-INPP5E D477N cilia (N = 30) and PI(4,5)P2.

White arrowheads point to the outer limits of PI(4,5)P2 staining at the ciliary tips (B). White arrows indicate extraciliary PI(4,5)P2 (B, D, and F). The scale bars represent 500 nm. See also Figures S3–S5.

MORM syndrome accumulates at the ciliary base and is absent from the ciliary tip (Jacoby et al., 2009). MORM INPP5E arises from loss of the CaaX domain, which targets proteins to the membrane, although it retains its catalytic activity (Jacoby et al., 2009). This highlights that INPP5E phosphatase activity is required at the ciliary tip.

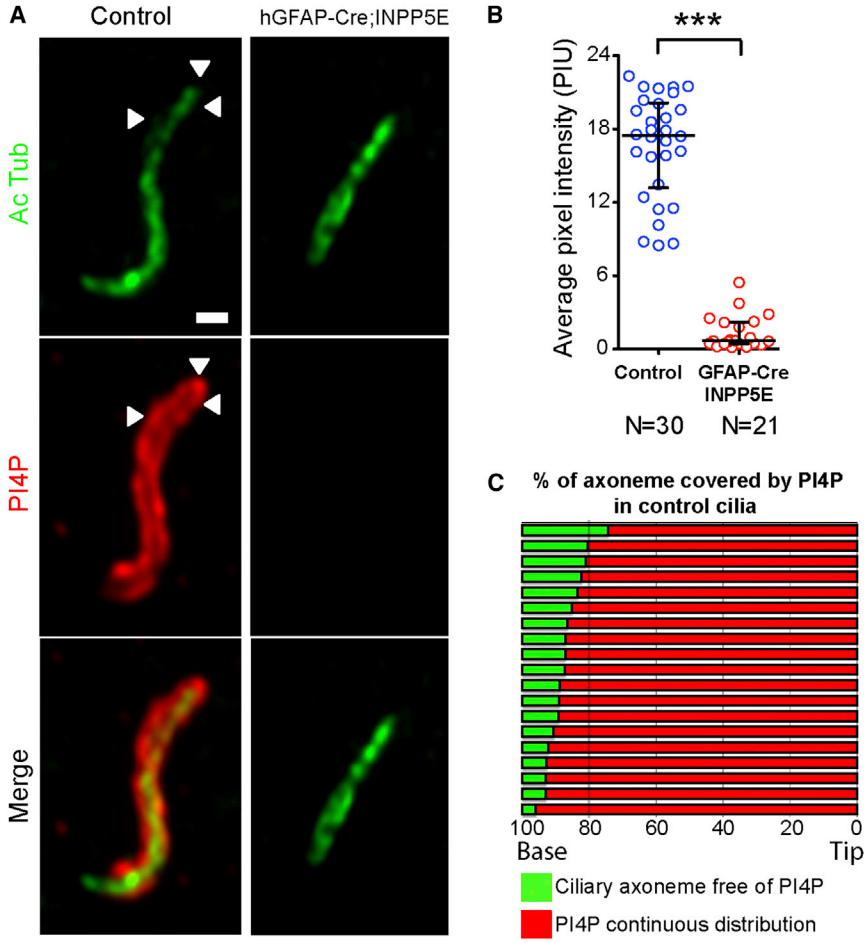

Figure 3. PI4P Regulation in Primary Cilia of Adherent NSCs

(A) Immunofluorescence for PI4P in control and *hGFAP-Cre;INPP5E*$^{flox/-}$ NSC cultures. White arrowheads point to the outer limits of PI4P staining at the ciliary tips. The scale bar represents 500 nm.

(B) Quantification of PI4P fluorescence intensity (1,000 pixel intensity units; PIUs). Each point represents a measurement from a single cilium; bars represent median fluorescence and interquartile ranges. Mann-Whitney test, ***$p < 0.0001$.

(C) Quantification of the percentage of the ciliary axoneme covered by PI4P in control cultures. Each bar represents a cilium (N = 19).

See also Figures S3–S5.

INPP5E Inactivation Leads to Ciliary Accumulation of TULP3 and the IFT-A Complex Protein IFT122

We next wondered whether PI(4,5)P2 accumulation and PI4P depletion could lead to redistribution of PIP-binding proteins. TULP3 has been described to bind primarily to PI(4,5)P2 (Mukhopadhyay et al., 2010), an interaction required to traffic a subset of GPCRs to the cilium (Mukhopadhyay et al., 2010). In control cilia, TULP3 staining revealed a weak and spotty pattern of staining, as previously described (Figure 4A) (Mukhopadhyay et al., 2010; Norman et al., 2009). Remarkably, TULP3 signal was stronger and continuously distributed around the ciliary axoneme of *hGFAP-Cre;INPP5E*$^{flox/-}$ primary cilia (Figures 4A and 4B). If TULP3 accumulates in cilia as the result of interaction with PI(4,5)P2, this interaction is expected to occur at the ciliary membrane. Membrane extraction greatly reduced TULP3 staining, confirming that TULP3 accumulated at the ciliary membrane of *hGFAP-Cre;INPP5E*$^{flox/-}$ cells (Figures S6B and S6C). Furthermore, we found no difference either in TULP3 transcript or protein levels between control and *hGFAP-Cre;INPP5E*$^{flox/-}$ cultures (Figures 4C and 4D), nor evidence of TULP3 redistribution or accumulation outside the cilia (Figure S7A), suggesting that TULP3 accumulation in cilia is not the result of increased transcription of TULP3 or overall protein accumulation of TULP3 but rather due to its recruitment at the ciliary membrane.

TULP3 accumulation was prevented by reexpression of the wild-type form of INPP5E in *Cre;INPP5E*$^{flox/-}$ cells (Figures 4E and 4F), whereas INPP5E D477N failed to prevent TULP3 accumulation in *Cre;INPP5E*$^{flox/-}$ cells (Figures 4G and 4H). Therefore, this shows that TULP3 accumulation upon INPP5E inactivation is the direct result of the loss of catalytic activity of INPP5E and not a consequence of lost interactions as a scaffolding protein.

TULP3 interacts via its N-terminal domain with intraflagellar transport (IFT-A) core complex proteins IFT122, WDR19, IFT140, THM1, and WDR35, and both this interaction and phosphoinositide-binding properties of TULP3 are required to traffic receptors to the cilia (Mukhopadhyay et al., 2010). In *hGFAP-Cre;INPP5E*$^{flox/-}$ primary cilia, we found an increase in IFT122 as compared to control cells (Figures 5A and 5B). Similar to TULP3, we could not detect any increase in IFT122 transcript nor protein levels in *hGFAP-Cre;INPP5E*$^{flox/-}$ cultures when compared to controls (Figures 5C and 5D), showing that IFT122 selectively accumulates within cilia and is not the result of increased transcription nor the consequence of global accumulation of IFT122. Thus, the PI(4,5)P2-binding protein TULP3 and its interacting partner IFT122 both accumulate in cilia following INPP5E inactivation.

Gpr161 Accumulates in Cilia upon INPP5E Inactivation, Leading to Increased Production of cAMP and Repression of Shh Signaling

Gpr161, a newly described repressor of Shh signaling, uses TULP3 and the IFT-A complex to be trafficked into the cilium (Mukhopadhyay et al., 2013). We therefore reasoned that accumulated TULP3 and IFT122 might affect Gpr161 trafficking and signaling into the cilium. We found that *hGFAP-Cre;INPP5E*$^{flox/-}$ cultures presented twice as many Gpr161-positive cilia compared to controls (Figure 6A). Similar to TULP3, we could not detect changes in Gpr161 total protein levels nor redistribution or accumulation of Gpr161 outside cilia upon INPP5E inactivation (Figure 6B; Figure S7B), showing that Gpr161

accumulation occurs selectively in cilia upon INPP5E inactivation. Reexpression of the wild-type form of INPP5E in *hGFAP-Cre;INPP5E*$^{flox/-}$ cultures reverted the percentage of Gpr161 cilia to wild-type percentages (Figure 6C), whereas INPP5E D477N failed to do so (Figure 6D), thus showing that INPP5E enzymatic activity is required to prevent Gpr161 from accumulating in cilia.

Gpr161 was evenly distributed continuously or in a spotty pattern along the ciliary axoneme in control cilia (Figures 6E and 6F) whereas in *hGFAP-Cre;INPP5E*$^{flox/-}$ cultures, Gpr161 staining was stronger and presented accumulations at the ciliary membrane, producing grossly distorted cilia on some occasions (Figures 6E and 6G). Gpr161 is internalized upon Shh stimulation in IMCD3 (inner medullar collecting duct) cells (Mukhopadhyay et al., 2013), thus relieving its negative effect on the pathway. Consistently, we found that the percentage of Gpr161-positive cilia decreased upon Shh stimulation in control cultures (Figure 6H). In contrast, Shh stimulation had no effect on *hGFAP-Cre;INPP5E*$^{flox/-}$ cultures, with the percentage of GPR161-positive cilia remaining unchanged (Figure 6H). Gpr161 internalization upon Shh stimulation was restored after reexpression of INPP5E WT in *hGFAP-Cre;INPP5E*$^{flox/-}$ cultures, whereas INPP5E D477N failed to do so (Figures 6I and 6J). Gpr161 has been described as increasing the production of cAMP via $G\alpha_s$ (Mukhopadhyay et al., 2013). Therefore, we investigated whether Gpr161 accumulation and resistance to internalization upon INPP5E inactivation might alter the levels of cAMP. We found a significant increase in cAMP produced upon forskolin stimulation in *hGFAP-Cre;INPP5E*$^{flox/-}$ cultures when compared to controls (Figure 7A). Gpr161 was reported to repress Shh response by increasing cAMP, thus activating protein kinase A (PKA), leading to formation of Gli3R and subsequent repression of Shh target transcription (Mukhopadhyay et al., 2013). Furthermore, Gpr161 has been detected in cultured mouse E16 hippocampal neurons and in the adult hippocampus (Mukhopadhyay et al., 2013). We thus hypothesized that Shh repression could explain the reduced hippocampal neurogenesis observed in *hGFAP-Cre;INPP5E*$^{flox/-}$ mice, because Shh signaling is known to control NSC proliferation in the DG (Han et al., 2008; Ihrie et al., 2011; Lai et al., 2003). Gli1 is not expressed in the absence of Shh but is upregulated upon Shh pathway activation and therefore used as a readout of Shh signaling (Wen et al., 2010). Consistent with our hypothesis, we found a significant decrease of Gli1 transcript levels in *INPP5E*$^{-/-}$ brains (Figure 7B) as well a reduced Gli1 response to Smoothened (Smo) agonist (SAG) stimulation in *hGFAP-Cre;INPP5E*$^{flox/-}$ cultures (Figure 7C), thus showing that INPP5E inactivation ultimately results in decreased Shh signaling.

Considering that INPP5E inactivation results in impaired Gpr161 trafficking, we checked whether the trafficking of other proteins involved in Shh response might be affected, thus providing an alternative explanation of the alterations we observed. In the absence of Shh ligand, Gpr161 is present in cilia whereas Smo is absent from cilia. Upon exposure to Shh, Gpr161 is removed from the cilia (Mukhopadhyay et al., 2013) and Smo accumulates within the cilia (Corbit et al., 2005). This triggers a chain of events, which ultimately results in the upregulation of Shh response genes (Haycraft et al., 2005; Kim et al., 2009). We stimulated cultured NSCs with SAG, and found that Smo significantly accumulated in cilia in both control and *hGFAP-Cre;INPP5E*$^{flox/-}$ cultures (Figure 7D; Figure S7C), thus showing that INPP5E inactivation does not impair Smo concentration in cilia, therefore not likely affecting Shh response due to a failure to accumulate Smo in cilia.

DISCUSSION

Here we provide the first report of PIPs at the primary ciliary membrane, and show how their regulation by INPP5E controls the ciliary trafficking of TULP3 and Gpr161. INPP5E inactivation results in accumulation of TULP3 and Gpr161 in cilia. Notably, not only is Gpr161 more abundant in cilia upon INPP5E inactivation but Gpr161 is also not internalized upon Shh stimulation, as occurs in controls (Figures 6A and 6H). Thus, its negative effect on Shh signaling is maintained even after ligand stimulation. cAMP levels were found to be increased upon INPP5E inactivation, supporting that Gpr161 accumulation results in increased cAMP production (Figure 7A). It is worth noting that PKA is a strong repressor of Shh signaling, because blocking PKA activity is enough to completely activate Shh gene transcription even in the absence of Shh (Hammerschmidt et al., 1996; Lepage et al., 1995; Tuson et al., 2011). On the other hand, treatment with forskolin, which activates PKA by raising cellular cAMP levels, abolishes Shh response (Tukachinsky et al., 2010). Thus, our model is that increased cAMP results from Gpr161 accumulation observed upon INPP5E inactivation, which directly activates PKA with subsequent reduction of the Shh response gene Gli1 (Figures 7E and 7F). Interestingly, polydactyly and exencephaly, features found in full INPP5E knockout embryos, have been found to result from aberrant Shh signaling (Lopez-Rios et al., 2012; Murdoch and Copp, 2010).

INPP5E inactivation in vivo results in ciliary defects and reduction in neurogenesis in the hippocampus (Figure S2), whereas proliferation assays in vitro revealed an increased BrdU incorporation in neurospheres (Figure 1D). These results would appear contradictory at first, but it is important to keep in mind that INPP5E degrades PI(3,4,5)P3 (Dyson et al., 2012), which activates AKT, thus promoting cell proliferation (Balla, 2013). We found that *INPP5E*$^{-/-}$ neurospheres presented an increased pAKT and BrdU incorporation (Figures 1D and 1E), likely as the result of PI(3,4,5)P3 accumulation. However, the physiological relevance of these data is difficult to interpret, because the amounts of mitogen (EGF) used in vitro for neurosphere cultures are likely much larger than the ones found in vivo. Thus, in vitro, this effect might counteract and overcome the negative effect on proliferation due to Shh pathway repression, via Gpr161 accumulation in neurospheres upon INPP5E inactivation.

In contrast to the PM, which contains levels of PI4P far in excess of those needed to support basal PI(4,5)P2 synthesis (Hammond et al., 2012), in primary cilia it appears that ciliary PI(4,5)P2 hydrolysis by INPP5E is the likely source of PI4P. Indeed, upon INPP5E inactivation, PI(4,5)P2 accumulates in cilia along with depletion of PI4P from the ciliary compartment (Figures 2B, 3A, and 3B), thus suggesting that PI(4,5)P2 is unable to be dephosphorylated to PI4P. This also suggests that there is no free movement of PI4P from the PM to the ciliary membrane. The ciliary compartment is subdivided into subcompartments. Projecting from the basal body is the transition zone (TZ), which constitutes the 0.5- to 1.0-μm basal part of the ciliary

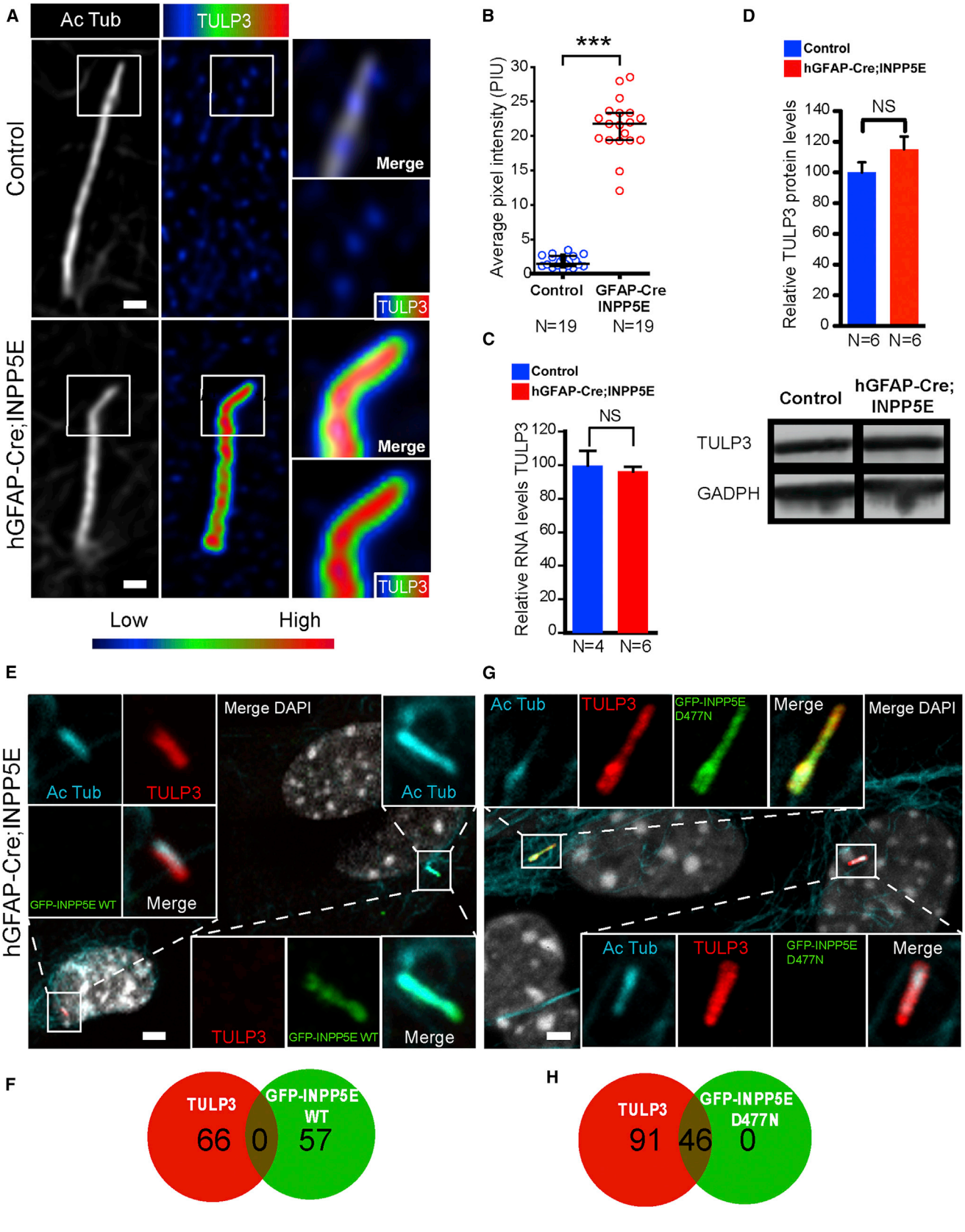

(legend on next page)

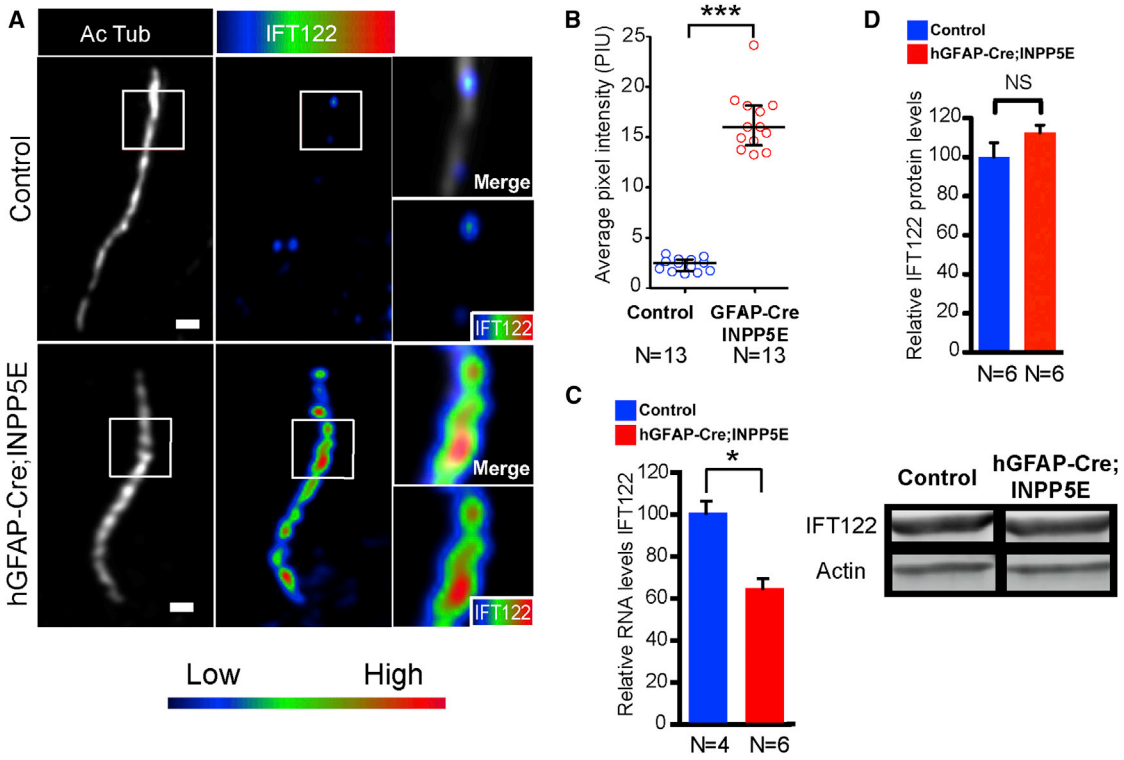

Figure 5. Ciliary Accumulation of IFT122 upon INPP5E Inactivation

(A) Immunofluorescence for IFT122 in control and *hGFAP-Cre;INPP5E*$^{flox/-}$ NSC cultures. The heat map shows IFT122 intensity. The scale bars represent 500 nm.

(B) Quantification of IFT122 fluorescence intensity (1,000 PIUs). Each point represents a measurement from a single cilium; bars represent median fluorescence and interquartile ranges. Mann-Whitney test, ***p < 0.0001.

(C) Quantitative PCR for IFT122 in control and *hGFAP-Cre;INPP5E*$^{flox/-}$ NSC cultures (N, number of independent cultures for each genotype; values are normalized to the control level). Unpaired t test, *p < 0.01.

(D) Immunoblotting for IFT122 in control and *hGFAP-Cre;INPP5E*$^{flox/-}$ NSC cultures. Unpaired t test, p = 0.1624.

axoneme (Reiter et al., 2012). The TZ serves as a ciliary gate isolating the cilium from the cell (Czarnecki and Shah, 2012; Garcia-Gonzalo et al., 2011). It is therefore tempting to speculate that this barrier might contribute to the isolation of PIPs in cilia from the PM, as shown by the absence of both PI(4,5)P2 and PI4P from the basal part of cilia (Figures 2C and 3C), where the TZ is located (Reiter et al., 2012). This subcompartmentalization would prevent movement of PIPs from the PM to the ciliary membrane, allowing a tight control of PIPs in cilia. It therefore appears that INPP5E function is to maintain low ciliary levels of PI(4,5)P2 in the ciliary compartment, allowing TULP3 trafficking within the cilium. Upon INPP5E inactivation, TULP3 will "stick" to the ciliary membrane, impairing its ciliary trafficking and consequently the movement of its interacting partners IFT122 and Gpr161. In addition to trafficking receptors to cilia, the IFT-A complex functions in the retrograde transport from the ciliary tip to the base. Mice lacking some IFT-A subunits have swollen and shorter primary cilia (Liem et al., 2012), due to accumulation of ciliary cargo at the ciliary tip. Therefore, the ciliary tip dilation found in hippocampal cells in *hGFAP-Cre;INPP5E*$^{flox/-}$ mice (Figures S2E,

Figure 4. Ciliary Accumulation of TULP3 upon INPP5E Inactivation

(A) Immunofluorescence for TULP3 in control and *hGFAP-Cre;INPP5E*$^{flox/-}$ NSC cultures. The heat map shows TULP3 intensity. The scale bars represent 500 nm.

(B) Quantification of TULP3 fluorescence intensity (1,000 PIUs). Each point represents a measurement from a single cilium; bars represent median fluorescence and interquartile ranges. Mann-Whitney test, ***p < 0.0001.

(C) Quantitative PCR for TULP3 in control and *hGFAP-Cre;INPP5E*$^{flox/-}$ NSC cultures (N, number of independent cultures for each genotype; values are normalized to the control level). Unpaired t test, p = 0.65. NS, not significant.

(D) Immunoblotting for TULP3 in control and *hGFAP-Cre;INPP5E*$^{flox/-}$ NSC cultures. Unpaired t test, p = 0.1864.

(E) Reexpression of GFP-INPP5E WT in *hGFAP-Cre;INPP5E*$^{flox/-}$ cultures. Note that GFP-INPP5E WT does not colocalize with accumulated TULP3. The scale bar represents 2 μm.

(F) Venn diagram depicting the absence of overlap between GFP-INPP5E WT (N = 57) and TULP3 (N = 66).

(G) Expression of GFP-INPP5E D477N in *hGFAP-Cre;INPP5E*$^{flox/-}$ cells. Note that GFP-INPP5E D477N does colocalize with accumulated TULP3. The scale bar represents 2 μm.

(H) Venn diagram depicting the overlap between GFP-INPP5E D477N cilia (N = 46) and TULP3.

See also Figures S6 and S7.

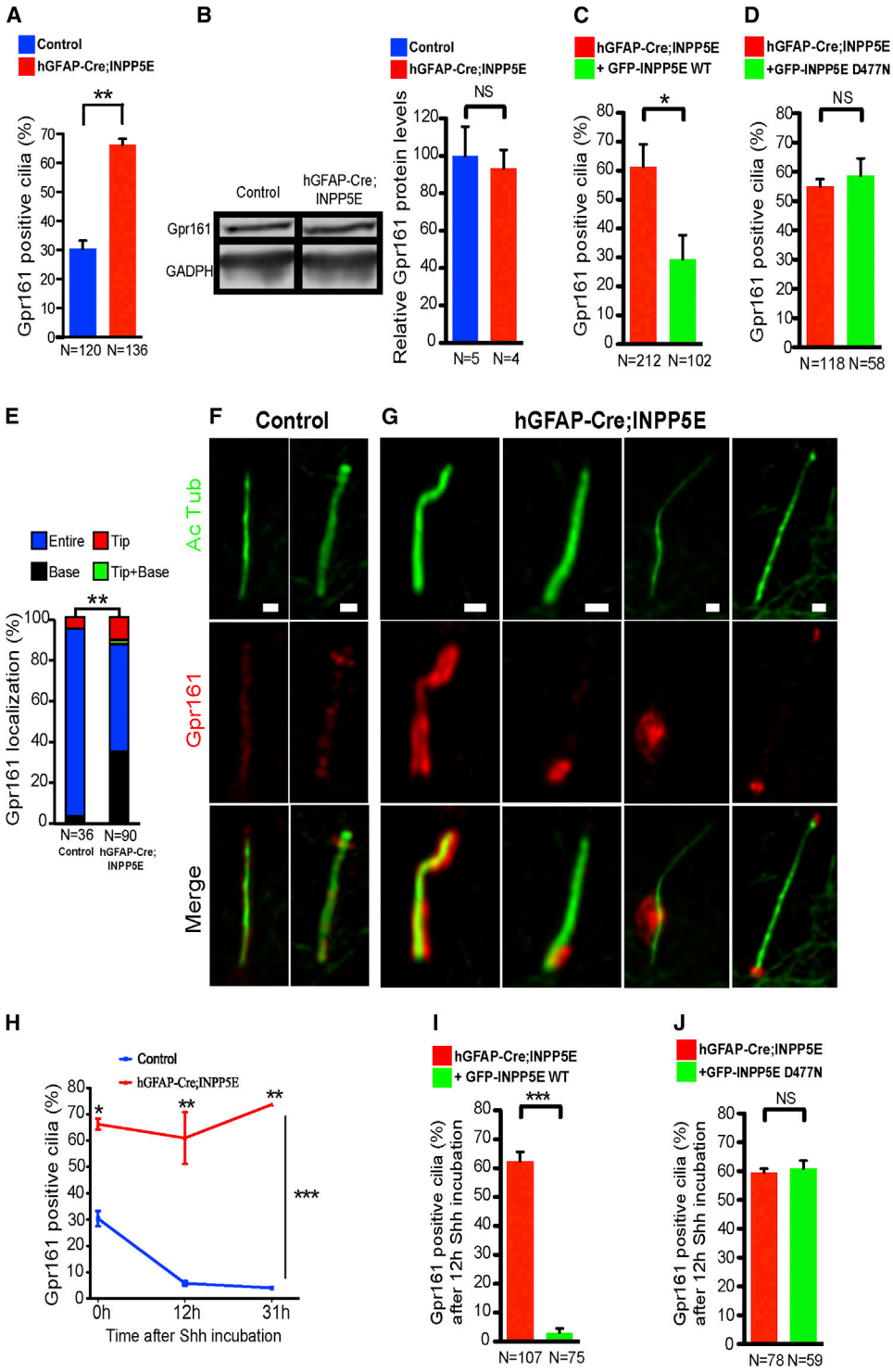

Figure 6. Effects of INPP5E Inactivation on Ciliary Trafficking of Gpr161

(A) Percentage of Gpr161-positive cilia in control and *hGFAP-Cre;INPP5E*$^{flox/-}$ NSCs coming from three different cultures. Unpaired t test, mean ± SEM, **$p < 0.001$.

(B) Immunoblotting for Gpr161 in control and *hGFAP-Cre;INPP5E*$^{flox/-}$ NSC cultures. Unpaired t test, $p = 0.7447$.

(C) Percentage of Gpr161-positive cilia following reexpression of GFP-INPP5E WT in *hGFAP-Cre;INPP5E*$^{flox/-}$ NSCs coming from three different cultures. Unpaired t test, mean ± SEM, *$p < 0.05$.

(D) Percentage of Gpr161-positive cilia following expression of GFP-INPP5E D477N in *hGFAP-Cre;INPP5E*$^{flox/-}$ NSCs coming from three different cultures. Unpaired t test, mean ± SEM, $p = 0.5910$.

(legend continued on next page)

S2H, and S2I) and the reduction in ciliary length in cultured NSCs (Figures 1F and 1G; Figure S3C) can be the result of compromised retrograde trafficking due to accumulation of IFT122 upon INPP5E inactivation.

Taken together, our findings provide mechanistic insights into the regulation of ciliary PIPs by INPP5E and its impact on ciliary function, and increase our understanding of ciliopathies, potentially opening intervention venues for their treatment.

EXPERIMENTAL PROCEDURES

Transgenic Mice

The generation and genotyping of *INPP5E*$^{flox/+}$ and *INPP5E*$^{flox/-}$ mice were described previously (Jacoby et al., 2009). Martin Theis from Bonn University kindly provided hGFAP-Cre mice, which were bred with *INPP5E*$^{flox/+}$ and *INPP5E*$^{flox/-}$ mice to produce conditional loss of INPP5E in neural stem cells (Han et al., 2008). *INPP5E*$^{flox/+}$ and *INPP5E*$^{flox/-}$ mice were generated on a 129 genetic background and backcrossed six times with C57BL/6 mice before use. hGFAP-Cre mice were generated in FVB/N mice and backcrossed with C57BL/6 mice. As previously reported for *CAGG-Cre-ERTM;INPP5E*$^{flox/-}$ (Jacoby et al., 2009), *hGFAP-Cre;INPP5E*$^{flox/+}$ and *INPP5E*$^{flox/-}$ mice were indistinguishable from control mice, and we therefore refer to them as controls. When relevant, the afternoon the vaginal plug was found was considered as embryonic day 0.5. All experiments were performed on mice according to the guidelines of the Animal Care Use and Review Committee of the Université Libre de Bruxelles.

Neural Stem Cell Culture and Treatments

Neurosphere culture and differentiation were performed as previously described (Rietze and Reynolds, 2006).

Adherent NSCs were cultured from newborn mice. Briefly, the lateral ventricular zone of newborn mice was dissected in Hank's medium (HBBS 1× without Ca^{2+} and Mg^{2+}) and digested for 1 hr with 0.25% trypsin and 0.01% DNase in Earle's balanced salt solution (EBSS 1× Ca^{2+} and Mg^{2+}), resuspended in DMEM containing 10% fetal bovine serum (FBS), 1% penicillin/streptomycin, plated in a culture flask, and maintained at 37°C in 5% CO_2. Cells were allowed to grow to confluence, and then rinsed with PBS, detached with 0.25% trypsin, and plated on polylysine-coated 10-mm coverslips, 90,000 cells/well on a 48-well culture plate. Cells were allowed to grow in DMEM with 10% FBS until full confluence. Upon confluence, medium was removed and replaced with serum-free DMEM to induce ciliation for 48 hr, and at this point coverslips were used for experiments. For Shh experiments, NSCs were treated with 300 ng/ml Rm-Shh-N terminus (R&D Systems) for 12 or 31 hr. For SAG experiments, NSCs were treated with 100 nM SAG (Millipore) for 4 (Figure 7D) or 48 hr (Figure 7C).

Materials

Plasmids, antibodies, and other reagents are listed in Supplemental Experimental Procedures.

Microscope Image Acquisition

All images, except Figures S2A and S2B, were obtained with a Zeiss LSM 780 laser-scanning microscope, 63× oil objective (numerical aperture [NA] 1.46) for in vitro studies and 40× water objective (NA 1.1) for ACIII staining in the DG (Figures S2D–S2I). Figures S2A and S2B were acquired using an Axio Imager M1 microscope equipped with a Zeiss AxioCam MRm digital camera with a 20× (NA 0.75) dry objective. High-resolution confocal microscopy ideal sampling was calculated using a Nyquist calculator (Scientific Volume Imaging) for each objective. Images were acquired sequentially for each fluorochrome in the order infrared, red, green, and blue to avoid crosstalk. Resulting images were deconvoluted using Huygens Professional software (4.2; Scientific Volume Imaging). Z planes containing structures of interest were projected into one picture, merged, and presented in interpolation display using ZEN 2010 D software (Carl Zeiss). For quantitative microscopy, images were taken under the same settings for both groups. Contrasts were adjusted identically for all figures.

cAMP Measurement

One million cells were seeded in 3.5-cm-diameter dishes with 2 ml culture medium. Cells were grown until confluence and starved for 48 hr. The medium was removed, and cells were washed and preincubated for 30 min in 1 ml Krebs-Ringer HEPES buffer (124 mM NaCl, 5 mM KCl, 1.25 mM $MgSO_4$, 1.45 mM $CaCl_2$, 1.25 mM KH_2PO_4, 25 mM HEPES [pH 7.4], 8 mM glucose, 0.5 g/L BSA) and then incubated for 1 hr with the phosphodiesterase inhibitor IBMX (1 mM) alone or in combination with the adenylyl cyclase activator forskolin (2 μM). The medium was removed and 1 ml of 0.1 M HCl was added. cAMP was measured in the dried cell extract by radioimmunoassay as previously described (Brooker et al., 1979).

Validation of the Specificity of Anti-PIP Antibodies and Staining

PI(4,5)P2

Neomycin, an aminoglycoside antibiotic, binds with high affinity to PI(4,5)P2, thus preventing an anti-PI(4,5)P2 antibody from binding to its target. Neomycin sulfate (1 mM; Enzo Life Sciences) was added to the blocking solution during PI(4,5)P2 staining.

PI4P

The specificity of the anti-PI4P antibody was verified by preabsorbing the antibody with POPC (Avanti Polar Lipids; 850457) liposomes containing 5% (mol/mol) dipalmitoyl PI4P (Echelon) for 1 hr at room temperature before incubation with samples (Hammond et al., 2009). Liposome preparation was done as described earlier (Hammond et al., 2009) with some modifications. Briefly, solubilized PI4P was dried under nitrogen gas in a glass tube and then resuspended in buffer containing 20 mM PIPES (pH 6.8), 137 mM NaCl, 2.7 mM KCl. Then, POPC was added to the solution and sonicated for 5 s five times to a final concentration of 140 μM total. Fresh liposomes were prepared the day of the experiment.

BrdU Incorporation In Vivo and In Vitro

Neurospheres in their third passage were dissociated into single cells, and 25,000 cells were seeded on 48-well plates containing 10-mm coverslips coated with poly-L-ornithine (Sigma). Cells were allowed to proliferate in medium containing EGF and, after 18 hr, the medium was removed and replaced with medium containing 10 μM BrdU for 1 hr. Cells were then fixed with 4% paraformaldehyde (20 min at room temperature), washed with PBS, and incubated for 15–17 min with 2 N HCl at 38.7°C, washed, and processed for immunocytochemistry using an anti-BrdU antibody.

For BrdU incorporation in the hippocampus, 10-week-old mice were injected intraperitoneally seven times at 2-hr intervals with BrdU (50 mg/kg body weight)

(E–G) Gpr161 localization in (F) control and (G) *hGFAP-Cre;INPP5E*$^{flox/-}$ NSCs. The scale bars represent 500 nm. (E) Gpr161 ciliary localization was scored as complete when it covered the whole ciliary axoneme, and as base, tip, or both when concentrated in those areas (N, number of Gpr161-positive cilia scored). χ^2 test, $^{**}p < 0.001$.

(H) Ciliary internalization of Gpr161 upon Shh stimulation (300 ng/ml) in control and *hGFAP-Cre;INPP5E*$^{flox/-}$ NSCs at 0 hr (control, N = 120; mutant, N = 136), 12 hr (control, N = 86; mutant, N = 91), and 31 hr (control, N = 49; mutant, N = 61) after Shh treatment. Two-way ANOVA, $^{***}p < 0.0001$ and Bonferroni post hoc test, mean ± SEM, $^{**}p < 0.001$, $^{*}p < 0.01$.

(I) Ciliary internalization of Gpr161 after a 12-hr Shh treatment upon reexpression of GFP-INPP5E WT in *hGFAP-Cre;INPP5E*$^{flox/-}$ NSCs coming from three different cultures. Unpaired t test, mean ± SEM, $^{***}p < 0.0001$.

(J) Ciliary internalization of Gpr161 after a 12-hr Shh treatment in GFP-INPP5E D477N transfected *hGFAP-Cre;INPP5E*$^{flox/-}$ NSCs coming from three different cultures. Unpaired t test, mean ± SEM, p = 0.6770.

See also Figure S7.

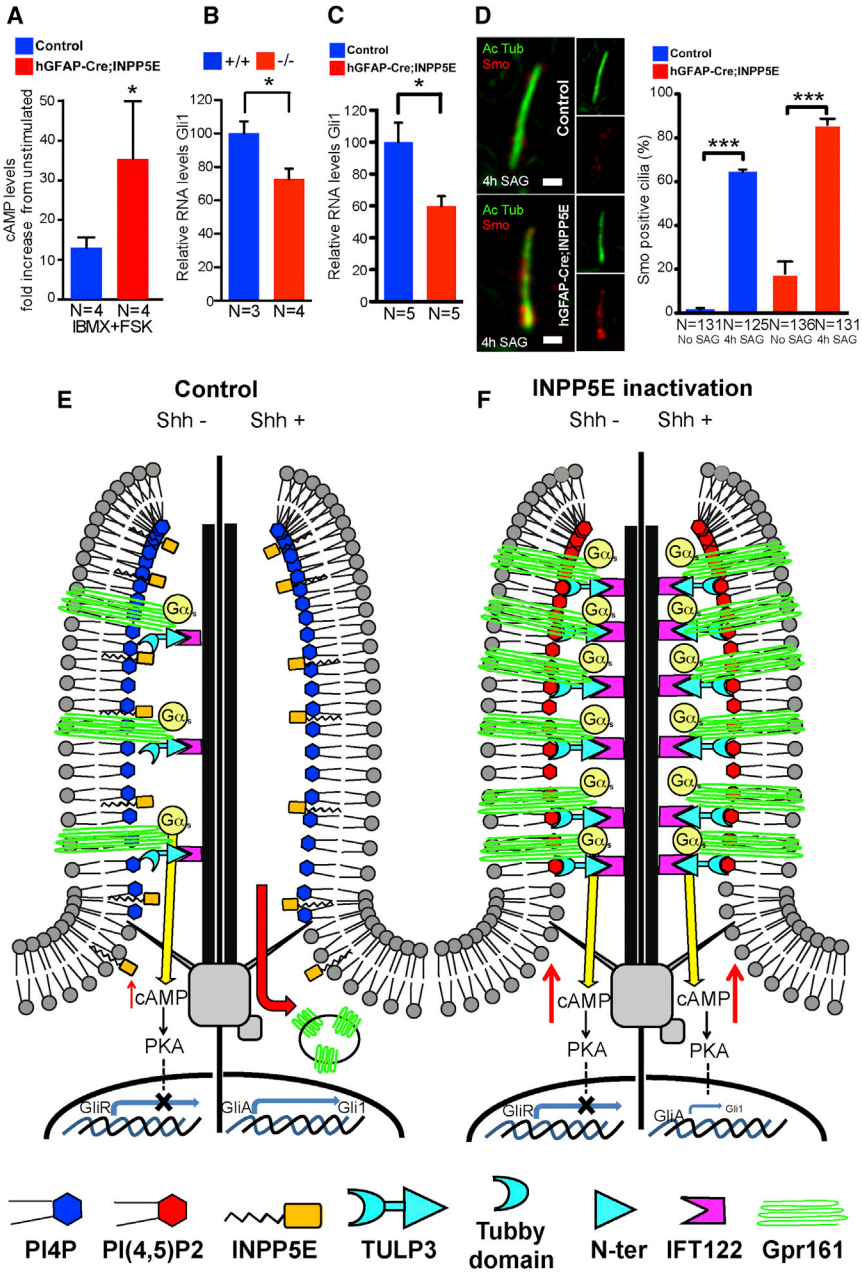

Figure 7. Effects of INPP5E Inactivation on Signaling Transduction and Shh Activation

(A) cAMP detection by radioimmunoassay in control and *hGFAP-Cre;INPP5E*$^{flox/-}$ NSCs. Cells were incubated with the adenylyl cyclase activator forskolin (FSK) (2 μM) and phosphodiesterase inhibitor IBMX (1 mM) for 1 hr. Values are presented as fold increase after IBMX + forskolin incubation compared to cultures incubated with IBMX alone. Mann-Whitney test, mean ± SEM, *p < 0.05.

(B) Gli1 transcript levels from *INPP5E*$^{+/+}$ and *INPP5E*$^{-/-}$ brains at E13.5. Unpaired t test, mean ± SEM, *p < 0.05.

(C) Gli1 transcript levels after a 48-hr stimulation by SAG (100 nM) of control and *hGFAP-Cre;INPP5E*$^{flox/-}$ cultures. Three different experiments coming from five different cultures were pooled. Values are normalized to the control level after SAG stimulation. Unpaired t test, *p < 0.05.

(D) Percentage of Smo-positive cilia in control and *hGFAP-Cre;INPP5E*$^{flox/-}$ cultures, before and after a 4-hr SAG stimulation, coming from three different cultures. Unpaired t test, mean ± SEM, control ***p < 0.0001, *hGFAP-Cre;INPP5E*$^{flox/-}$ ***p = 0.0004. The scale bars represent 500 nm.

(E and F) Model for the role of INPP5E in TULP3 and IFT-A complex trafficking. Control cells (E): INPP5E maintains PI4P as the main PIP in primary cilia. TULP3 traffics Gpr161 into the cilium via interaction with the IFT-A complex. Ciliary Gpr161 activates cAMP production via the $G\alpha_s$ subunit, leading to the repression of transcription of Shh-targeted genes. Upon Shh stimulation, Gpr161 is internalized, thus releasing its negative effect on the Shh pathway and allowing Shh-mediated gene transcription. Upon INPP5E inactivation (F), PI(4,5)P2 accumulates at the ciliary membrane and PI(4,5)P2 recruits TULP3 to the ciliary membrane. This results in TULP3 accumulation along with its interacting partner IFT122, part of the IFT-A complex. Gpr161 is hindered in its internalization, probably by direct interaction with the TULP3-IFT122 complex, resulting in an increased amount of Gpr161 in cilia. Upon Shh stimulation, GPR161 is not internalized, thus preserving its activation of cAMP production, which in turn results in repression of Shh-targeted genes.

See also Figure S7.

and sacrificed 1 hr after the last injection by intracardiac perfusion with PBS and 4% paraformaldehyde. BrdU exposure was done as previously described (Tattersfield et al., 2004). Immunostained cells were counted in at least six sections from each mouse at comparable rostrocaudal levels.

Method of Randomization Used to Assign Samples and Collect and Process Data

Mice used for in vivo or in vitro studies came from the same litter and were genotyped before being used. For in vitro studies, cultured cells coming from the mouse of interest were grown in a flask and later seeded on coverslips. For confocal microscopy, coverslips of interest were analyzed on the basis of the ciliary marker Ac Tub; every ciliated cell, which appeared on nonoverlapping fields, was acquired. For some ciliary markers (i.e., PI(4,5)P2), which were also expressed on the plasma membrane, only cilia in which the ciliary marker was clearly distinguishable from that of the PM were considered, to avoid misinterpretation.

Ciliated Cell Quantification and Ciliary Length Measurement

Acetylated α-tubulin was used as a ciliary marker and 4′,6-diamidino-2-phenylindole (DAPI) was used for counterstaining. Three nonoverlapping fields were acquired at 40× on an Axio Imager M1 microscope totaling 500–1,000 cells per culture coming from three different NSC cultures. Counting was done in ImageJ (NIH). For length measurement, only cilia whose emergency points and tips were distinguishable were measured along the ciliary axoneme using ZEN 2010 D.

Fluorescence Intensity Quantification

Quantification was done using the Advanced Weka Segmentation plugin for ImageJ. Laser intensity and gain were set in the brightest sample below saturation, and this was kept during acquisition for both groups. Confocal images were deconvoluted and split into separate 16-bit tiff files for TULP3 or IFT122 and acetylated α-tubulin. A binary mask was created (using acetylated tubulin as a reference for cilium location) and used to extract the mean pixel intensity

per sample. Data were analyzed by Microsoft Excel spreadsheet software and plotted using Prism software (GraphPad).

Statistics

To determine the significance between two groups, indicated in the figures by asterisks, comparisons were made using a two-tailed Mann-Whitney test, Student's two-tailed t test, two-way ANOVA followed by Bonferroni post hoc test, or χ^2 test and plotted using Microsoft Excel or Prism software.

SUPPLEMENTAL INFORMATION

Supplemental Information includes Supplemental Experimental Procedures and seven figures and can be found with this article online at http://dx.doi.org/10.1016/j.devcel.2015.06.016.

AUTHOR CONTRIBUTIONS

M.C. and S.N.S. designed and analyzed the experiments and wrote the manuscript. M.C. generated *hGFAP-Cre;INPP5E*$^{flox/-}$ mice and performed all experiments, other than S.E., who ran TULP3/IFT122 qPCRs, J.V.S., who assisted with cAMP measurements, and A.d.K.d., who assisted in generating the phosphatase-dead form of INPP5E. S.S. made *INPP5E*$^{flox/-}$ and *INPP5E*$^{+/-}$ mice available and discussed the experiments. All authors commented on the manuscript.

ACKNOWLEDGMENTS

We thank Martin Theis for the hGFAP-Cre mice, Jonathan Eggenschwiler for the anti-TULP3 antibody, Yasunori Kanaho for the anti-PIP5K antibodies, Genentech for the Gpr161 antibody, Christophe Erneux for discussions on PIPs, Claude Massart for assistance with cAMP measurements, Williams Elong Edimo for advice on liposome preparation, Delphine Houtteman for running Gli1 qPCRs, Souad Laghmari for genotyping, and Frederic Bollet-Quivogne and Jean-Marie Vanderwinden (LiMiF) for the Weka fragmentation tool and comments on microscopy. M.C. was supported by a Télévie grant from FRS-FNRS and by Van Buuren funds. A.d.K.d. is "Maître de Recherche" of the FRS-FNRS. This study was supported by FMRE-Belgium, FRS-FNRS (Belgium), Interuniversity Attraction Pole (IUAP-P7/10) from Belgian Federal Scientific Affairs, and Action de Recherche Concertée (CFWB, AUWB 08/13 ULB 8).

Received: June 5, 2014
Revised: March 31, 2015
Accepted: June 18, 2015
Published: July 16, 2015

REFERENCES

Balla, T. (2013). Phosphoinositides: tiny lipids with giant impact on cell regulation. Physiol. Rev. *93*, 1019–1137.

Berbari, N.F., O'Connor, A.K., Haycraft, C.J., and Yoder, B.K. (2009). The primary cilium as a complex signaling center. Curr. Biol. *19*, R526–R535.

Bielas, S.L., Silhavy, J.L., Brancati, F., Kisseleva, M.V., Al-Gazali, L., Sztriha, L., Bayoumi, R.A., Zaki, M.S., Abdel-Aleem, A., Rosti, R.O., et al. (2009). Mutations in INPP5E, encoding inositol polyphosphate-5-phosphatase E, link phosphatidyl inositol signaling to the ciliopathies. Nat. Genet. *41*, 1032–1036.

Breunig, J.J., Sarkisian, M.R., Arellano, J.I., Morozov, Y.M., Ayoub, A.E., Sojitra, S., Wang, B., Flavell, R.A., Rakic, P., and Town, T. (2008). Primary cilia regulate hippocampal neurogenesis by mediating sonic hedgehog signaling. Proc. Natl. Acad. Sci. USA *105*, 13127–13132.

Brooker, G., Harper, J.F., Terasaki, W.L., and Moylan, R.D. (1979). Radioimmunoassay of cyclic AMP and cyclic GMP. Adv. Cyclic Nucleotide Res. *10*, 1–33.

Corbit, K.C., Aanstad, P., Singla, V., Norman, A.R., Stainier, D.Y., and Reiter, J.F. (2005). Vertebrate Smoothened functions at the primary cilium. Nature *437*, 1018–1021.

Czarnecki, P.G., and Shah, J.V. (2012). The ciliary transition zone: from morphology and molecules to medicine. Trends Cell Biol. *22*, 201–210.

Danilov, A.I., Gomes-Leal, W., Ahlenius, H., Kokaia, Z., Carlemalm, E., and Lindvall, O. (2009). Ultrastructural and antigenic properties of neural stem cells and their progeny in adult rat subventricular zone. Glia *57*, 136–152.

Doetsch, F., Caillé, I., Lim, D.A., García-Verdugo, J.M., and Alvarez-Buylla, A. (1999). Subventricular zone astrocytes are neural stem cells in the adult mammalian brain. Cell *97*, 703–716.

Doetsch, F., Petreanu, L., Caille, I., Garcia-Verdugo, J.M., and Alvarez-Buylla, A. (2002). EGF converts transit-amplifying neurogenic precursors in the adult brain into multipotent stem cells. Neuron *36*, 1021–1034.

Dyson, J.M., Fedele, C.G., Davies, E.M., Becanovic, J., and Mitchell, C.A. (2012). Phosphoinositide phosphatases: just as important as the kinases. Subcell. Biochem. *58*, 215–279.

Franco, I., Gulluni, F., Campa, C.C., Costa, C., Margaria, J.P., Ciraolo, E., Martini, M., Monteyne, D., De Luca, E., Germena, G., et al. (2014). PI3K class II α controls spatially restricted endosomal PtdIns3P and Rab11 activation to promote primary cilium function. Dev. Cell *28*, 647–658.

Garcia-Gonzalo, F.R., Corbit, K.C., Sirerol-Piquer, M.S., Ramaswami, G., Otto, E.A., Noriega, T.R., Seol, A.D., Robinson, J.F., Bennett, C.L., Josifova, D.J., et al. (2011). A transition zone complex regulates mammalian ciliogenesis and ciliary membrane composition. Nat. Genet. *43*, 776–784.

Hammerschmidt, M., Bitgood, M.J., and McMahon, A.P. (1996). Protein kinase A is a common negative regulator of Hedgehog signaling in the vertebrate embryo. Genes Dev. *10*, 647–658.

Hammond, G.R., Dove, S.K., Nicol, A., Pinxteren, J.A., Zicha, D., and Schiavo, G. (2006). Elimination of plasma membrane phosphatidylinositol (4,5)-bisphosphate is required for exocytosis from mast cells. J. Cell Sci. *119*, 2084–2094.

Hammond, G.R., Schiavo, G., and Irvine, R.F. (2009). Immunocytochemical techniques reveal multiple, distinct cellular pools of PtdIns4P and PtdIns(4,5)P(2). Biochem. J. *422*, 23–35.

Hammond, G.R., Fischer, M.J., Anderson, K.E., Holdich, J., Koteci, A., Balla, T., and Irvine, R.F. (2012). PI4P and PI(4,5)P2 are essential but independent lipid determinants of membrane identity. Science *337*, 727–730.

Han, Y.G., Spassky, N., Romaguera-Ros, M., Garcia-Verdugo, J.M., Aguilar, A., Schneider-Maunoury, S., and Alvarez-Buylla, A. (2008). Hedgehog signaling and primary cilia are required for the formation of adult neural stem cells. Nat. Neurosci. *11*, 277–284.

Haycraft, C.J., Banizs, B., Aydin-Son, Y., Zhang, Q., Michaud, E.J., and Yoder, B.K. (2005). Gli2 and Gli3 localize to cilia and require the intraflagellar transport protein polaris for processing and function. PLoS Genet. *1*, e53.

Higginbotham, H., Guo, J., Yokota, Y., Umberger, N.L., Su, C.Y., Li, J., Verma, N., Hirt, J., Ghukasyan, V., Caspary, T., and Anton, E.S. (2013). Arl13b-regulated cilia activities are essential for polarized radial glial scaffold formation. Nat. Neurosci. *16*, 1000–1007.

Ihrie, R.A., Shah, J.K., Harwell, C.C., Levine, J.H., Guinto, C.D., Lezameta, M., Kriegstein, A.R., and Alvarez-Buylla, A. (2011). Persistent sonic hedgehog signaling in adult brain determines neural stem cell positional identity. Neuron *71*, 250–262.

Ishikawa, H., Thompson, J., Yates, J.R., 3rd, and Marshall, W.F. (2012). Proteomic analysis of mammalian primary cilia. Curr. Biol. *22*, 414–419.

Jacoby, M., Cox, J.J., Gayral, S., Hampshire, D.J., Ayub, M., Blockmans, M., Pernot, E., Kisseleva, M.V., Compère, P., Schiffmann, S.N., et al. (2009). INPP5E mutations cause primary cilium signaling defects, ciliary instability and ciliopathies in human and mouse. Nat. Genet. *41*, 1027–1031.

Jensen, J.B., and Parmar, M. (2006). Strengths and limitations of the neurosphere culture system. Mol. Neurobiol. *34*, 153–161.

Kim, J., Kato, M., and Beachy, P.A. (2009). Gli2 trafficking links Hedgehog-dependent activation of Smoothened in the primary cilium to transcriptional activation in the nucleus. Proc. Natl. Acad. Sci. USA *106*, 21666–21671.

Kim, Y.J., Hernandez, M.L., and Balla, T. (2013). Inositol lipid regulation of lipid transfer in specialized membrane domains. Trends Cell Biol. *23*, 270–278.

Kobayashi, T., and Dynlacht, B.D. (2011). Regulating the transition from centriole to basal body. J. Cell Biol. *193*, 435–444.

Kong, A.M., Horan, K.A., Sriratana, A., Bailey, C.G., Collyer, L.J., Nandurkar, H.H., Shisheva, A., Layton, M.J., Rasko, J.E., Rowe, T., and Mitchell, C.A. (2006). Phosphatidylinositol 3-phosphate [PtdIns3P] is generated at the plasma membrane by an inositol polyphosphate 5-phosphatase: endogenous PtdIns3P can promote GLUT4 translocation to the plasma membrane. Mol. Cell. Biol. *26*, 6065–6081.

Kwon, I.S., Lee, K.H., Choi, J.W., and Ahn, J.Y. (2010). PI(3,4,5)P3 regulates the interaction between Akt and B23 in the nucleus. BMB Rep *43*, 127–132.

Lai, K., Kaspar, B.K., Gage, F.H., and Schaffer, D.V. (2003). Sonic hedgehog regulates adult neural progenitor proliferation in vitro and in vivo. Nat. Neurosci. *6*, 21–27.

Lepage, T., Cohen, S.M., Diaz-Benjumea, F.J., and Parkhurst, S.M. (1995). Signal transduction by cAMP-dependent protein kinase A in *Drosophila* limb patterning. Nature *373*, 711–715.

Liem, K.F., Jr., Ashe, A., He, M., Satir, P., Moran, J., Beier, D., Wicking, C., and Anderson, K.V. (2012). The IFT-A complex regulates Shh signaling through cilia structure and membrane protein trafficking. J. Cell Biol. *197*, 789–800.

Lopez-Rios, J., Speziale, D., Robay, D., Scotti, M., Osterwalder, M., Nusspaumer, G., Galli, A., Holländer, G.A., Kmita, M., and Zeller, R. (2012). GLI3 constrains digit number by controlling both progenitor proliferation and BMP-dependent exit to chondrogenesis. Dev. Cell *22*, 837–848.

Mukhopadhyay, S., and Jackson, P.K. (2011). The tubby family proteins. Genome Biol. *12*, 225.

Mukhopadhyay, S., Wen, X., Chih, B., Nelson, C.D., Lane, W.S., Scales, S.J., and Jackson, P.K. (2010). TULP3 bridges the IFT-A complex and membrane phosphoinositides to promote trafficking of G protein-coupled receptors into primary cilia. Genes Dev. *24*, 2180–2193.

Mukhopadhyay, S., Wen, X., Ratti, N., Loktev, A., Rangell, L., Scales, S.J., and Jackson, P.K. (2013). The ciliary G-protein-coupled receptor Gpr161 negatively regulates the Sonic hedgehog pathway via cAMP signaling. Cell *152*, 210–223.

Murdoch, J.N., and Copp, A.J. (2010). The relationship between sonic Hedgehog signaling, cilia, and neural tube defects. Birth Defects Res. A Clin. Mol. Teratol. *88*, 633–652.

Niswender, K.D., Gallis, B., Blevins, J.E., Corson, M.A., Schwartz, M.W., and Baskin, D.G. (2003). Immunocytochemical detection of phosphatidylinositol 3-kinase activation by insulin and leptin. J. Histochem. Cytochem. *51*, 275–283.

Norman, R.X., Ko, H.W., Huang, V., Eun, C.M., Abler, L.L., Zhang, Z., Sun, X., and Eggenschwiler, J.T. (2009). Tubby-like protein 3 (TULP3) regulates patterning in the mouse embryo through inhibition of Hedgehog signaling. Hum. Mol. Genet. *18*, 1740–1754.

Reiter, J.F., Blacque, O.E., and Leroux, M.R. (2012). The base of the cilium: roles for transition fibres and the transition zone in ciliary formation, maintenance and compartmentalization. EMBO Rep. *13*, 608–618.

Rietze, R.L., and Reynolds, B.A. (2006). Neural stem cell isolation and characterization. Methods Enzymol. *419*, 3–23.

Rohatgi, R., Milenkovic, L., and Scott, M.P. (2007). Patched1 regulates hedgehog signaling at the primary cilium. Science *317*, 372–376.

Santagata, S., Boggon, T.J., Baird, C.L., Gomez, C.A., Zhao, J., Shan, W.S., Myszka, D.G., and Shapiro, L. (2001). G-protein signaling through tubby proteins. Science *292*, 2041–2050.

Seri, B., García-Verdugo, J.M., McEwen, B.S., and Alvarez-Buylla, A. (2001). Astrocytes give rise to new neurons in the adult mammalian hippocampus. J. Neurosci. *21*, 7153–7160.

Tao, R., Gong, J., Luo, X., Zang, M., Guo, W., Wen, R., and Luo, Z. (2010). AMPK exerts dual regulatory effects on the PI3K pathway. J. Mol. Signal. *5*, 1.

Tattersfield, A.S., Croon, R.J., Liu, Y.W., Kells, A.P., Faull, R.L., and Connor, B. (2004). Neurogenesis in the striatum of the quinolinic acid lesion model of Huntington's disease. Neuroscience *127*, 319–332.

Tukachinsky, H., Lopez, L.V., and Salic, A. (2010). A mechanism for vertebrate Hedgehog signaling: recruitment to cilia and dissociation of SuFu-Gli protein complexes. J. Cell Biol. *191*, 415–428.

Tuson, M., He, M., and Anderson, K.V. (2011). Protein kinase A acts at the basal body of the primary cilium to prevent Gli2 activation and ventralization of the mouse neural tube. Development *138*, 4921–4930.

Vieira, O.V., Gaus, K., Verkade, P., Fullekrug, J., Vaz, W.L., and Simons, K. (2006). FAPP2, cilium formation, and compartmentalization of the apical membrane in polarized Madin-Darby canine kidney (MDCK) cells. Proc. Natl. Acad. Sci. USA *103*, 18556–18561.

Watt, S.A., Kular, G., Fleming, I.N., Downes, C.P., and Lucocq, J.M. (2002). Subcellular localization of phosphatidylinositol 4,5-bisphosphate using the pleckstrin homology domain of phospholipase C delta1. Biochem. J. *363*, 657–666.

Wei, H.C., Rollins, J., Fabian, L., Hayes, M., Polevoy, G., Bazinet, C., and Brill, J.A. (2008). Depletion of plasma membrane PtdIns(4,5)P2 reveals essential roles for phosphoinositides in flagellar biogenesis. J. Cell Sci. *121*, 1076–1084.

Wei, Q., Zhang, Y., Li, Y., Zhang, Q., Ling, K., and Hu, J. (2012). The BBSome controls IFT assembly and turnaround in cilia. Nat. Cell Biol. *14*, 950–957.

Wen, X., Lai, C.K., Evangelista, M., Hongo, J.A., de Sauvage, F.J., and Scales, S.J. (2010). Kinetics of hedgehog-dependent full-length Gli3 accumulation in primary cilia and subsequent degradation. Mol. Cell. Biol. *30*, 1910–1922.

Zhang, L., Mao, Y.S., Janmey, P.A., and Yin, H.L. (2012). Phosphatidylinositol 4, 5 bisphosphate and the actin cytoskeleton. Subcell. Biochem. *59*, 177–215.